Processing and Application of Ceramics 15 [3] (2021) 279–287
https://doi.org/10.2298/PAC2103279D

Influence of YTS addition on structural and electrical properties of PZT-based ceramics

Yasmina Djoudi[1,*], Fares Kahoul[2,3], Louanes Hamzioui[2,3], Abderrezak Guemache[2]

[1]*Université de Ouargla, Département Génie des Procédés, Laboratoire de Dynamique, Interaction et Réactivité des Systèmes, Ouargla 30000, Algeria*
[2]*Université de M'Sila, Département Socle Commun ST, Faculté de Technologie, M'Sila 28000, Algeria*
[3]*Université de Biskra, Département de Chimie, Laboratoire de Chimie Appliquée, B.P. 145, RB-Biskra 07000, Algeria*

Received 12 December 2020; Received in revised form 27 March 2021; Received in revised form 15 July 2021; Accepted 23 August 2021

Abstract

Perovskite solid solution (1-x)Pb($Zr_{0.52}Ti_{0.48}$)O_3-xY($Ta_{1/2}Sb_{1/2}$)O_3 ceramics (abbreviated as PZT-YTS, where x = 0, 0.01, 0.02, 0.03, 0.04 and 0.05) were synthesized by conventional solid state method. The phase structure, microstructure and corresponding electrical properties were studied. X-ray diffraction and Raman analyses show that tetragonal phase structure was obtained in all ceramics at room temperature. Scanning electron micrographs of the samples show uniform grain distribution and grain growth inhibition with the increase of doping content. The dielectric permittivity, dissipation factor, electromechanical coupling factor, Young modulus, mechanical quality factor, piezoelectric charge constant, actual density and piezoelectric voltage constant, for the ceramics with x = 0.04 were: ε_r = 714.9, tan δ = 0.03345, K_P = 0.635, $Y = 10.528 \times 10^{10}$ N/m^2, Q_m = 622.254, $d_{31} = 74.738 \times 10^{-12}$ C/N, ρ_a = 7.67 g/cm^3 and $g_{31} = 10.477 \times 10^{-3}$ m·V/N, respectively, which are optimal in comparison to other studied samples.

Keywords: *PZT ceramics, sintering, SEM, piezoelectric properties, resistivity*

I. Introduction

$Pb(Zr_{1-x}Ti_x)O_3$ (PZT) ceramics, with perovskite (ABO_3) structure, exhibit excellent ferroelectric and piezoelectric properties and high Curie temperature (T_C). This make them effective for use in a wide range of applications, including actuators, transducers, acoustic devices and resonators, and military sonars as well as in ultrasonic welding, ultrasonic cutting, gas ignition, ferroelectric random-access memory (FeRAM), microelectromechanical systems (MEMS), etc. [1–8].

$Pb(Zr_{1-x}Ti_x)O_3$ has excellent piezoelectric properties for a composition x of approximately 0.48, which corresponds to the morphotropic phase boundary (MPB) where the tetragonal (Ti-rich) and rhombohedral (Zr-rich) phases coexist [9–11]. It has been observed that the properties of these ceramics are very sensitive to the composition fluctuation near the MPB, sintering temperature and dopant concentration. In order to achieve a high degree of molecular mixing, chemical homogeneity, control of stoichiometry, low calcination and sintering temperature, various chemical methods [12] have been used for the synthesis of these compounds. However, processing of PZT ceramics by a solid-solution mixing process has the advantages of convenient preparation and low cost [13]. It is well-known that the performance of piezoelectric ceramics can be improved by doping [14,15]. In PZT, donor doping or doping with higher valence ions on either the A- or B-site has been shown to result in a "softening" which is typically characterized by increase in piezoelectric activity, dielectric constant (ε_r) and dielectric loss (tan δ), as well as decrease in the coercive field (E_c) and mechanical quality factor (Q_m). Alternatively, acceptor doping or doping with lower valence cations results in the formation of compensating oxygen vacancies. Defect associates and dipoles consisting of acceptor ions and compensat-

*Corresponding author: tel: +213 55 473 49 87,
e-mail: *djoudiyasmina1@gmail.com* (Y. Djoudi)
fares.kahoul@univ-msila.dz (F. Kahoul)

ing oxygen vacancies can be formed which then align along the polarization axes which lead to a stabilization of the domain configuration. Consequently, the material exhibits "hardening" which is characterized by a reduction in piezoelectric activity, a decrease in ε_r and $\tan\delta$ as well as an increase in Q_m and E_c.

The piezoelectric ceramics are usually obtained by doping with several cations and then made into polycrystalline bulk by high-temperature sintering and solid-state reaction [16–19]. In the next step, the piezoelectric ceramics are polarized in silicon oil under high voltage which makes them highly piezoelectric, thus the piezoelectric ceramics can realize successful transformation between mechanical and electrical energy. The dopants can be divided into three main categories: i) donor doping, such as La^{3+}, Bi^{3+}, Nd^{3+} doped in A sites, Nb^{5+} in B sites [20–22], ii) acceptor doping, such as Mn^{2+}, Fe^{3+}, Al^{3+}, Dy^{3+}, Er^{3+} doped in B sites [23–26], iii) isovalent doping, such as Sr^{2+}, Ca^{2+}, Ba^{2+} in A sites, Sr^{4+} in B sites [27,28]. PZT doping with donor ions, such as Y^{3+} at A-site and Ta^{5+}, Sb^{5+} at B-site, reduces the concentration of intrinsic oxygen vacancies created due to PbO evaporation and compensates the hole formed due to lead vacancies, which in turn increases bulk resistance of the sample. The PZT ceramics modified with Y exhibits good dielectric and piezoelectric responses (PZT (52/48) + 2 at.% Y has ε_{max} = 2100, P_r = 26 μC/cm^2) [29]. Similarly, PZT modified with Ta and Sb exhibits the improved piezoelectric properties (PZT + 0.1 at.% Sb has ε_{max} = 2663, P_r = 1.26 μC/cm^2, T_C = 415.0 °C, whereas PZT + 0.1 at.% Ta has ε_{max} = 5893, P_r = 2.69 μC/cm^2, T_C = 388.5 °C) [30].

The perovskite phase formation in PZT ceramics generally takes place at elevated temperatures (at 1180 °C) [31], however, at high firing temperatures, significant amount of PbO will be lost due to its volatilization. Unfortunately, in conventional solid state synthesis route, the PbO loss is inevitable due to the multiple steps required for phase formation, beginning with calcinations and subsequent extreme sintering temperatures [32]. The excess PbO powder is intentionally added during the batch preparation of Pb-based ceramics to prevent composition shifting and to compensate the loss of PbO during heating cycles. Additionally, it is added to enhance densification by forming a PbO-rich liquid phase during the sintering process [31–34].

In this study, perovskite ceramics containing Y^{3+}, Ta^{5+} and Sb^{5+} ions, i.e. (1-x)Pb($Zr_{0.52}Ti_{0.48}$)O_3-xY($Ta_{1/2}Sb_{1/2}$)O_3 (PZT-YTS, x = 0, 0.01, 0.02, 0.03, 0.04 and 0.05) were prepared by conventional solid state sintering method. Microstructure and temperature-dependent dielectric and piezoelectric properties of these materials were investigated in detail.

II. Experimental procedure

All used oxides Pb_3O_4 (99.9%), TiO_2 (98.9%), ZrO_2 (99.9%), Y_2O_3 (99.8%), Sb_2O_5 (99.6%) and Ta_2O_5 (99.8%), were obtained from Aldrich chemicals. The stoichiometric amounts in the designated (1-x)Pb($Zr_{0.52}Ti_{0.48}$)O_3-xY($Ta_{1/2}Sb_{1/2}$)O_3 (where x = 0, 0.01, 0.02, 0.03, 0.04 and 0.05) compositions were mixed in ethanol (solvent) by a magnetic stirrer for 2 h and then dried in the oven at 80 °C. After milling (RETSCH PM-200, Germany) in tungsten carbide bowls with tungsten carbide balls in ethyl alcohol medium for 6 h, the resulting slurry was dried and the powder was calcined in alumina crucible at 800 °C for 2 h. The calcined powders were milled for the second time and subsequently compacted into pellets using polyvinyl alcohol (PVA) binder under a pressure of 98 MPa. The pellets were sintered at 1180 °C for 2 h in a closed alumina crucibles at a heating rate of 5 °C/min and natural cooling in the furnace (70 °C/h), in the presence of $PbZrO_3$ powder to prevent PbO loss during the high temperature sintering. The sintered pellets were electroded by high-purity silver particle paste and fired at 750 °C, before any electrical measurements.

Room temperature powder X-ray patterns were recorded on a Philips diffractometer using CuK_α radiation with a wave-length of λ_1 = 1.54056 Å in the angle range of 10° ≤ 2θ ≤ 70° with a 10 s counting time for each step of 0.02°. The Archimedes method was used for measuring the densities of the sintered samples. Microstructure of the ceramics was examined by the scanning electron microscopy (FESEM, Quanta 250FEG, USA). The Raman spectra were recorded using a Raman spectrometer from Princeton Instruments (HORIBA HR800).

Dielectric properties were measured at 1 kHz using an LCR meter (800 GWI, LTD) in the temperature range from 25 to 450 °C with a heating rate of 1 °C/min. The ceramics were poled at 120 °C in silicone oil under an electric field of 30–40 kV/cm for 45 min using a poling system (Rek RK2674A, HYJH-3YY/20 kV). For investigation of the piezoelectric properties, the resonant and anti-resonant frequencies were measured by an impedance analyzer (Agilent 4294A).

III. Results and discussion

3.1. XRD patterns and Raman spectra

Room-temperature XRD patterns of the PZT-YTS ceramics containing different amounts of YTS (x = 0, 0.01, 0.02, 0.03, 0.04 and 0.05) sintered at 1180 °C for 2 h are shown in Fig. 1. The XRD patterns confirm that all the PZT-YTS powders have pure single-phase perovskite structure without any peaks of pyrochlore phases for all compositions. The peak splitting of 002 and 200 reflections around 2θ = 45° suggested that the crystal structure of the PZT-YTS ceramics was tetragonal. With the YTS content increase, the increased intensity of the XRD peaks indicates that the crystallinity becomes better.

The XRD results indicate that Y^{3+} (0.106 nm), Ta^{5+} (0.068 nm) and Sb^{5+} (0.062 nm) dopants diffuse in the

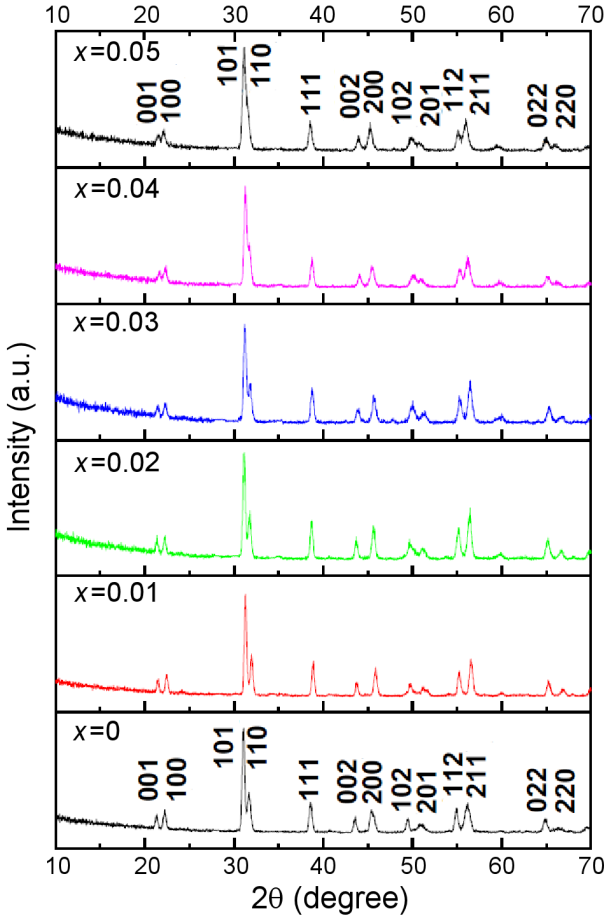

Figure 1. XRD patterns of 2θ = 10°–70°, of the PZT-YTS ceramics sintered at 1180 °C

Table 1. Theoretical density ρ_{th}, actual density ρ_a and relative density ρ_r of the PZT-YTS ceramics

x	ρ_{th} [g/cm^3]	ρ_a [g/cm^3]	ρ_r [% TD]
0	8.04	7.32	91.04
0.01	7.95	7.37	92.7
0.02	7.93	7.63	96.21
0.03	7.9	7.65	96.83
0.04	7.85	7.67	97.7
0.05	7.88	7.66	97.20

PZT lattice to form a homogeneous solid solutions. In view of its ionic radius and chemical valance, it is reasonable that Ta^{5+} and Sb^{5+} ions occupy the B-site of Zr^{4+} (0.072 nm)/Ti_4^+ (0.060 nm) ions, and Y^{3+} occupies the A-site of Pb^{2+} (0.119 nm) ion.

Using the Archimedes method the actual density of the PZT-YTS ceramics was measured and the calculation of the theoretical density is based on the knowledge of the lattice parameter data. The theoretical density, actual density and relative density of the (1-x)Pb($Zr_{0.52}Ti_{0.48}$)O_3-xY($Ta_{1/2}Sb_{1/2}$)O_3 (x = 0, 0.01, 0.02, 0.03, 0.04 and 0.05) ceramics samples are shown in Table 1. According to the results, the actual density shows a maximum (7.67 g/cm^3) for a value of x = 0.04, where a relative density of 97.7% has been reached.

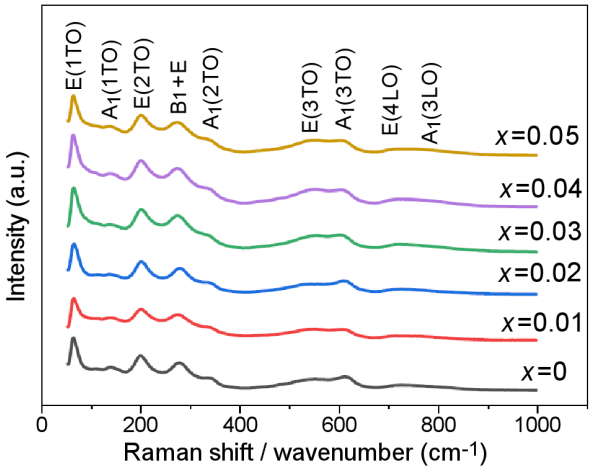

Figure 2. Raman spectra of (1-x)Pb($Zr_{0.52}Ti_{0.48}$)O_3-xY($Ta_{1/2}Sb_{1/2}$)O_3 ceramics at room temperature

Raman spectroscopy is sensitive to the symmetry of crystalline structures and is, therefore, a suitable technique to study the structure and phase evolution of the prepared ceramics. Room-temperature Raman spectra recorded in the 50–1000 cm^{-1} wave number range for the (1-x)Pb($Zr_{0.52}Ti_{0.48}$)O_3-xY($Ta_{1/2}Sb_{1/2}$)O_3 ceramics for compositions x = 0, 0.01, 0.02, 0.03, 0.04 and 0.05 are depicted in Fig. 2. The experimental Raman spectra are basically in good agreement with the published data which confirms that steady PZT-YTS phase has already formed in these sintered ceramics [35–37]. There were seven obvious peaks, which were located at about 63, 137, 199, 276, 333, 554, 611, 718 and 755 cm^{-1}. Each peak represents the Raman active vibrational mode for a given sample, suggesting that the samples are pure and do not contain any compositional inhomogeneity.

The assignments of Raman active modes and Raman shifts are listed in Table 2. The presented values confirm that the PZT-YTS samples are free from the inhomogeneity and contain tetragonal phase that occurred in all the ceramics.

3.2. Microstructure of ceramics

Figure 3 shows the SEM images of the PZT-YTS ceramics with different YTS contents sintered at 1180 °C for 2 h. The microstructures of the PZT-YTS ceramics are well crystallized with homogeneous grain size distributions and very dense. The average grain size of the ceramics is influenced by the change in YTS contents. The grain boundary migration speed is improved after adding YTS which causes a disproportionate grain distribution, so the grain growth of the PZT-YTS ceramics is accelerated due to the liquid phases involved.

The decrease of grain size can be explained by the partial substitution of PZT by YTS resulting in an increased average mobility of the ions, which induced a slow inter-diffusion movement via the grain boundary, preventing the formation of necks between the grains as well as its growth and thus inhibiting the growth of the

Table 2. The assignments of Raman active modes, Raman shifts and phase structure for PZT-YTS ceramics at room temperature [9,38–43]

Raman shift [cm^{-1}]	Active modes	Assignments	Phase structure
63	E(1TO)	Pb-BO_3 stretching	Tetragonal or Rhombohedral
137	A_1(1TO)	Cation-(BO_3) lattice modes	Tetragonal
199	E(2TO)	O–B–O bending	Tetragonal
276	B_1 + E	B-localized	Tetragonal or Rhombohedral
333	A_1(2TO)	O–B–O stretching	Tetragonal or Rhombohedral
554	E(3TO)	O–B–O bending	Tetragonal
611	A_1(3TO)	O–B–O bending	Tetragonal
718	E(4LO)	O–B–O bending	Tetragonal
755	A_1(3LO)	B–O stretching	Tetragonal

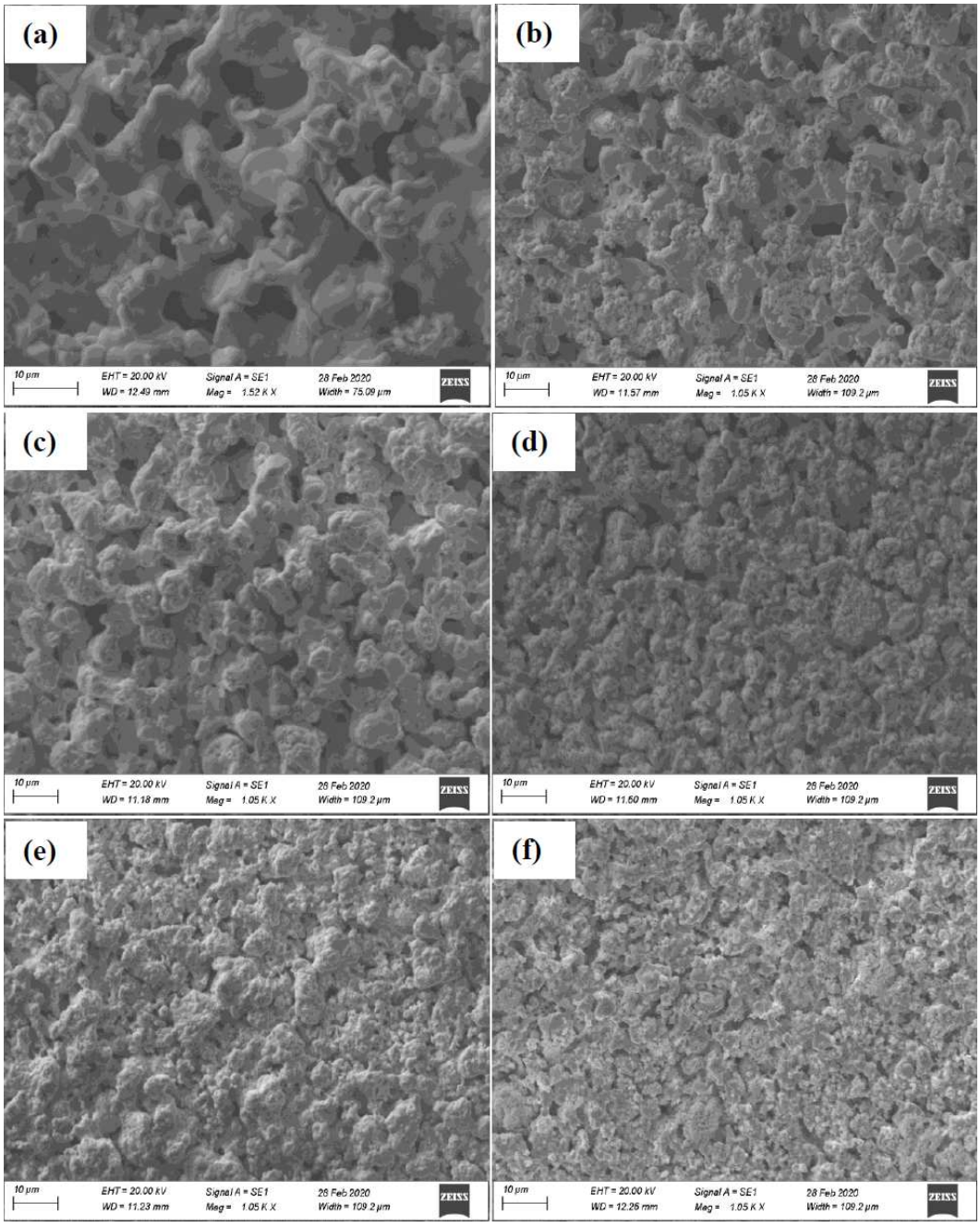

Figure 3. SEM micrographs of fracture surfaces of PZT-YTS ceramics as a function of YTS contents, *x*: a) 0, b) 0.01, c) 0.02, d) 0.03, e) 0.04 and f) 0.05

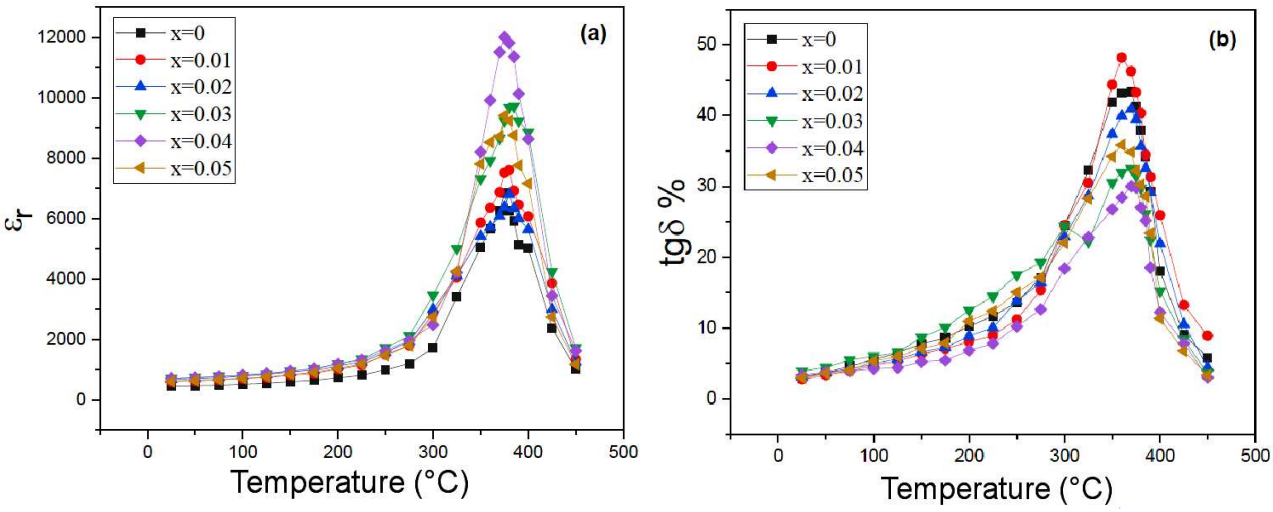

Figure 4. Dielectric permittivity, ε_r (a) and dissipation factor, tan δ (b) as functions of temperature for PZT-YTS ceramics at 1 kHz

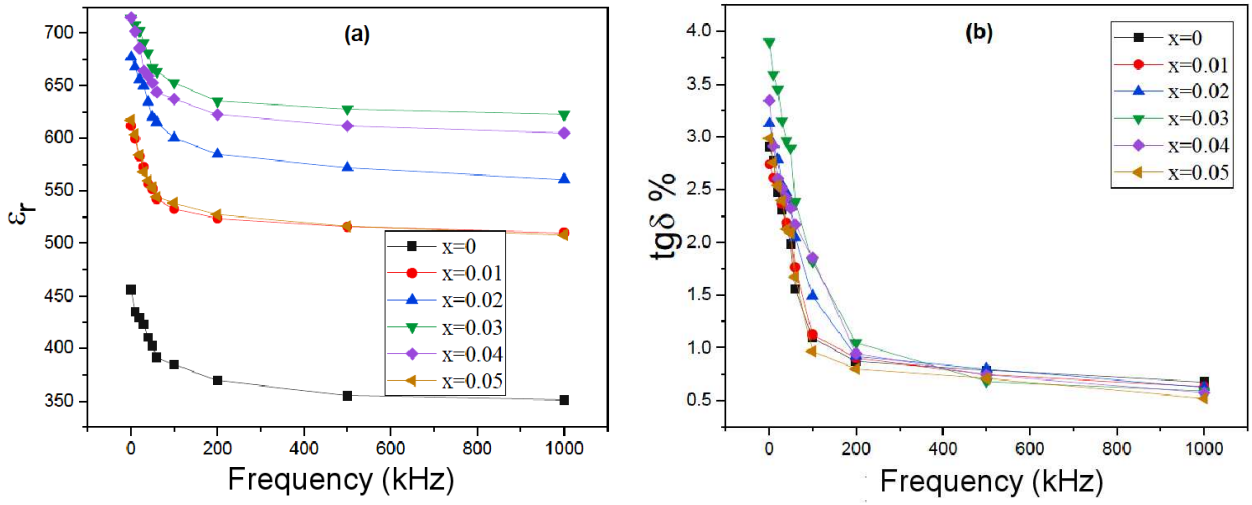

Figure 5. Variation of dielectric permittivity ε_r (a) and dissipation factor, tan δ (b) of PZT-YTS ceramics (with different compositions, x = 0, 0.01, 0.02, 0.03, 0.04 and 0.05) with frequency

grains. Secondly, it is found that PZT-YTS ceramics becomes denser as Y^{3+}, Ta^{5+} and Sb^{5+} content increases.

3.3. Electrical properties

Figures 4a and 4b show the temperature dependence of the dielectric permittivity (ε_r) and dissipation factor (tan δ) of the (1-x)Pb($Zr_{0.52}Ti_{0.48}$)O_3-xY($Ta_{1/2}Sb_{1/2}$)O_3 ceramics with various x values (0, 0.01, 0.02, 0.03, 0.04 and 0.05) measured at 1 kHz in the test temperature range from 25–450 °C. Figure 4a shows that there is phase transition in the dielectric-temperature response for all ceramic samples at tetragonal-cubic (the Curie temperature, T_C) phase transition temperature. The Curie temperature was observed to increase from 375 to 385 °C as x was increased from 0 to 0.003, then decreases to 375 °C for $x \geq 0.04$. A diffuse phase transition is observed for all the PZT-YTS ceramic samples which results in a wide maximum range for the change of dielectric permittivity with temperature.

From Fig. 4b, it is observed that the dissipation factor (tan δ) gives all the signs of transitions clearly. At high temperature, tan δ increases suddenly which could be due to the generation of space charge at high temperature.

Dielectric permittivity (ε_r) and dissipation factor (tan δ) versus frequency plots for the PZT-YTS ceramics (x = 0–0.05) are shown in Fig. 5. One can see from Fig. 5a that the dielectric permittivity of all the samples decreases sharply with the increase of frequency in the low frequency range, while the dielectric permittivity tends to be stable at higher frequencies. This can be attributed to the different responses of various polarization mechanisms in different frequency regions, and the polarization relaxation is ascribed to this phenomenon [44,45].

At low frequency, all types of polarizations (ionic, electronic, dipole and space charges polarization) contribute to the dielectric permittivity. At higher frequencies, the easy depolarization of dipoles that exist at weakly bonded interfaces and boundary regions results

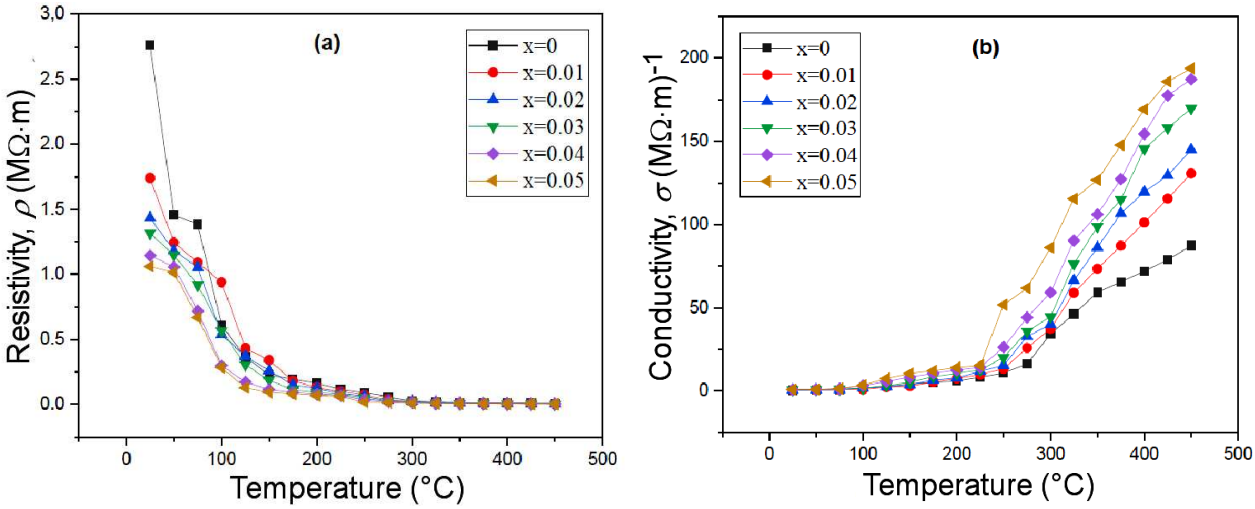

Figure 6. Temperature dependent: a) resistivity (ρ) and b) conductivity (σ) of (1-x)Pb($Zr_{0.52}Ti_{0.48}$)O_3-xY($Ta_{1/2}Sb_{1/2}$)O_3 (where x = 0–0.05) ceramics at frequency of 1 kHz

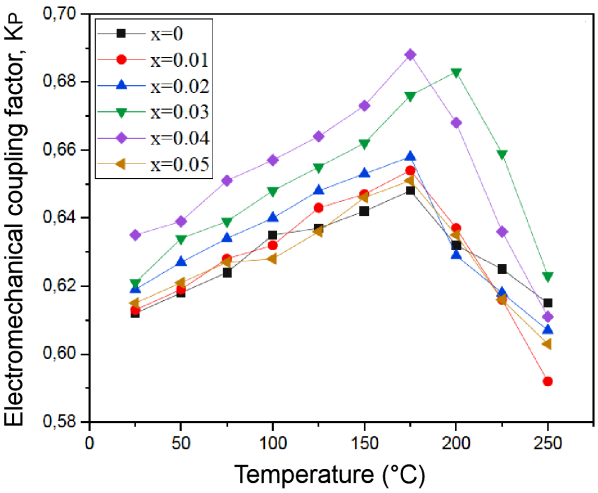

Figure 7. Dependence of $K_P(T)$ for (1-x)Pb($Zr_{0.52}Ti_{0.48}$)O_3-xY($Ta_{1/2}Sb_{1/2}$)O_3 ceramics (where x = 0–0.05)

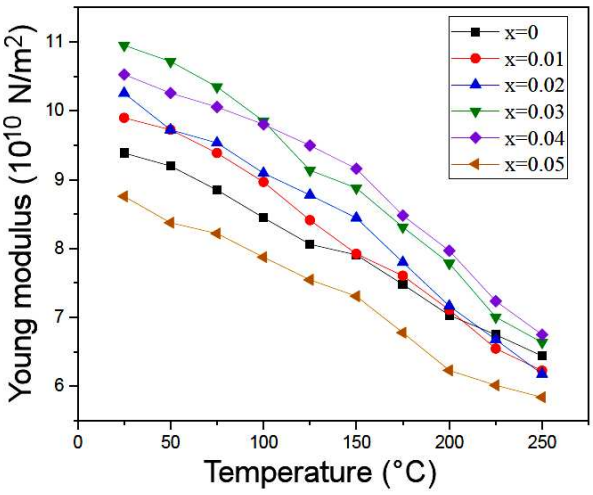

Figure 8. Dependence of $Y(T)$ for (1-x)Pb($Zr_{0.52}Ti_{0.48}$)O_3-xY($Ta_{1/2}Sb_{1/2}$)O_3 ceramics (where x = 0–0.05)

in small value of dielectric permittivity. At higher frequency, only the orientation polarization contributes to the dielectric permittivity.

Figure 5b shows that in all samples tan δ decreases with increasing frequencies. As such, tan δ represents contribution of conduction loss due to ions migration, ions jump, also ion polarization and vibration loss.

Figures 6a and 6b show the change in resistivity ρ and conductivity σ with the temperature measured at 1 kHz for the PZT-YTS ceramics with x = 0, 0.01, 0.02, 0.03, 0.04 and 0.05. With the increase in temperature and YTS contents a gradual decrease in resistivity can be seen, indicating thermally activated process and an increase in conductivity due to the hopping of charge carriers from one preferable site to another.

Figure 7 shows the temperature dependence of the electromechanical coupling factor K_P of the PZT-YTS ceramics with various YTS contents. The K_P increases initially and then decreases drastically with the increasing temperature. The defect dipoles on domain walls can act as pinning points which prevent the domain from movement and hence decrease the K_P value [46].

The temperature dependence of Young modulus Y of the PZT-YTS ceramics is shown in Fig. 8. With an increase in temperature, there is a marked decrease in the value of the Young modulus Y in a continued way. The decrease of this factor could be explained by the attractive forces that prevent vibration dipoles [47].

Figure 9 shows the temperature dependence of the mechanical quality factor Q_m of the PZT-YTS ceramics with various YTS contents. The Q_m decreases as temperature increases. The mechanical quality factor is defined as the reciprocal of the internal friction. Vacant Pb sites support the movement of domain walls and increase the internal friction within the ceramics.

Table 3 exhibits the measured values for physical properties of PZT-YTS ceramics according to the variation of YTS at room temperature.

Table 3. Physical properties of PZT-YTS ceramics as a function of YTS substitution

x	ε_r	$\tan\delta$ [%]	ρ [MΩ·m]	σ [MΩ^{-1}·m^{-1}]	K_P	Y [10^{10} N/m^2]	Q_m	d_{31} [10^{-12} C/N]	g_{31} [10^{-3} m·V/N]
0	455.845	2.905	2.762	0.362	0.612	9.386	451.155	70.319	10.346
0.01	611.847	2.741	1.739	0.575	0.613	9.897	484.025	72.414	10.467
0.02	677.271	3.125	1.434	0.697	0.619	10.256	661.611	73.428	10.524
0.03	714.089	3.897	1.317	0.759	0.621	10.95	689.875	76.534	10.564
0.04	714.945	3.345	1.145	0.873	0.635	10.528	622.254	74.738	10.477
0.05	617.406	2.985	1.061	0.942	0.615	8.758	473.785	71.887	10.185

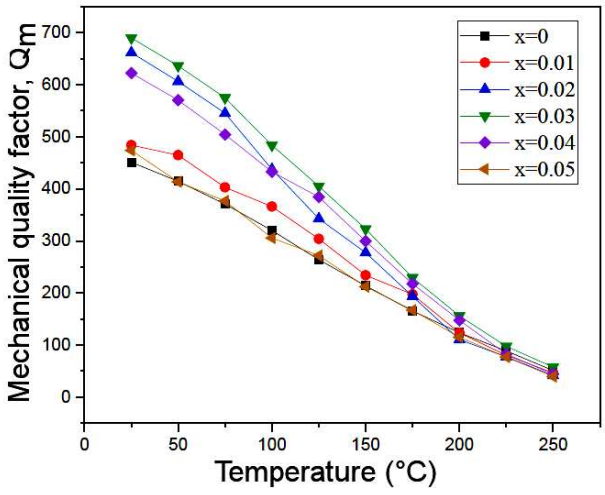

Figure 9. Dependence of $Q_m(T)$ for (1-x)Pb($Zr_{0.52}Ti_{0.48}$)O_3-xY($Ta_{1/2}Sb_{1/2}$)O_3 ceramics (where x = 0–0.05)

IV. Conclusions

(1-x)Pb($Zr_{0.52}Ti_{0.48}$)O_3-xY($Ta_{1/2}Sb_{1/2}$)O_3 ceramics (where x = 0–0.05) were fabricated via the conventional solid-state reaction method. The phase structure, microstructure and electrical properties were systematically investigated. XRD and Raman spectra revealed that the PZT-YTS ceramics possesses pure perovskite structure with tetragonal symmetry. The grain size was decreased and the density was increased with addition of YTS. The conductivity at 20–450 °C is mainly due to oxygen vacancies and it also increases with YTS addition. As a result, the optimized values of ε_r (714.945), $\tan\delta$ (0.03345), K_P (0.635), Y (10.528 × 10^{10} N/m^2), Q_m (622.254), d_{31} (74.738 × 10^{-12} C/N), actual density (7.67 g/cm^3) and g_{31} (10.477 × 10^{-3} m·V/N) were obtained for x = 0.04.

References

1. L.D. Vuong , P.D. Gio, N.D. V. Quang, T.D. Hieu, T.P. Nam, "Development of 0.8Pb($Zr_{0.48}Ti_{0.52}$)O_3–0.2Pb[($Zn_{1/3}Nb_{2/3}$)$_{0.625}$($Mn_{1/3}Nb_{2/3}$)$_{0.375}$]O_3 ceramics for high-intensity ultrasound applications", *J. Electron. Mater.*, **47** (2018) 5944–5951.
2. X. Huang, J. Zeng, X. Ruan, L. Zheng, G. Li, "Structure, electrical, and thermal expansion properties of PZnTe-PZT ternary system piezoelectric ceramics", *J. Am. Ceram. Soc.*, **101** (2018) 274–282.
3. C.H. Hong, H.P. Kim, B.Y. Choi, H.S. Han, J.S. Son, C.W. Ahn, W. Jo, "Lead-free piezoceramics - Where to move on?", *J. Materiomics*, **2** (2016) 1–24.
4. P. Kour, S.K. Pradhan, P. Kumar, S.K. Sinha, M. Kar, "Study of ferroelectric and piezoelectric properties on Ca doped PZT ceramics", *Mater. Today Proc.*, **4** (2017) 5727–5733.
5. Y. Yue, Q. Zhang, R. Nie, P. Yu, Q. Chen, H. Liu, J. Zhu, D. Xiao, H. Song, "Influence of sintering temperature on phase structure and electrical properties of 0.55Pb($Ni_{1/3}Nb_{2/3}$)O_3–0.45Pb($Zr_{0.3}Ti_{0.7}$)O_3 ceramics", *Mater. Res. Bull.*, **92** (2017) 123–128.
6. M.A. Qaiser, A. Hussain, Y. Xu, Y. Wang, Y. Wang, Y. Yang, G. Yuan, "CuO added $Pb_{0.92}Sr_{0.06}Ba_{0.02}(Mg_{1/3}Nb_{2/3})_{0.25}(Ti_{0.53}Zr_{0.47})_{0.75}O_3$ ceramics sintered with Ag electrodes at 900 °C for multilayer piezoelectric actuator", *Chin. Phys. B*, **26** (2017) 037702–037707.
7. L.D. Vuong, P.D. Gio, N.T. Tho, T.V. Chuong, "Relaxor ferroelectric properties of PZT-PZN-PMnN ceramics", *India. J. Eng. Mater. Sci.*, **20** (2013) 555–560.
8. S. Zhang, F. Li, X. Jiang, J. Kim, J. Luo, X. Geng, "Advantages and challenges of relaxor-$PbTiO_3$ ferroelectric crystals for electroacoustic transducers - A review", *Prog. Mater. Sci.*, **68** (2015) 1–66.
9. A. Kumar, S.K. Mishra, "Effects of Sr^{2+} substitution on the structural, dielectric, and piezoelectric properties of PZT-PMN ceramics", *Int. J. Miner. Metal Mater.*, **21** (2014) 175–180
10. L. Hamzioui, F. Kahoul, A. Boutarfaia, "The effect of Nb_2O_5 addition on the structural, dielectric and piezoelectric properties of $Pb_{0.98}Ba_{0.02}[(Zr_{0.52}Ti_{0.48})_{0.98}(Cr^{3+}_{0.5},Ta^{5+}_{0.5})_{0.02}]$ ceramics", *Energ. Proced.*, **74** (2015) 198–204.
11. F. Kahoul, L. Hamzioui, A. Guemache, M. Aillerie, A. Boutarfaia, "Dielectric, phase structure, microstructure, and dielectric properties of (1-x)Pb($Zr_{0.50}Ti_{0.50}$)O_3–xBa($W_{2/3}Mn_{1/3}$)O_3 ceramics", *Ferroelectrics*, **572** (2021) 229–237.
12. F. Kahoul, L. Hamzioui, Z. Necira, A. Boutarfaia, "Effect of sintering temperature on the electromechanical properties of (1-x)Pb(Zr_yTi_{1-y})O_3-xSm($Fe^{3+}_{0.5}$,$Nb^{5+}_{0.5}$)O_3 ceramics", *Energ. Proced.*, **36** (2013) 1050–1059.
13. T. Stevenson, D.G. Martin, P.I. Cowin, A. Blumfield, A.J. Bell, T.P. Comyn, P.M. Weaver, "Piezoelectric materials for high temperature transducers and actuators", *J. Mater. Sci. Mater. Electron.*, **26** (2015) 9256–9267.
14. Q. Liao, X. Chen, X. Chu, F. Zeng, D. Guo, "Effect of Fe doping on the structure and electric properties of relaxor type BSPT-PZN piezoelectric ceramics near the morphotropic phase boundary", *Sens. Actuato. A Phys.*, **201** (2013) 222–229.
15. H.W. Zhu, D.Y. Zheng, X.J. Wang, L. Yang, C. Fang, Z.H. Peng, "Effects of Ta_2O_5 addition on relaxation behavior and electric properties of PMS-PNN-PZT ceramics",

J. Mater. Sci. Mater. Electron., **29** (2018) 16864–16871.
16. Z. Liu, "Current investigation of doping modification of PZT", *J. Funct. Mater.*, **4** (2015) 04009–04014.
17. M.A. Qaiser, A. Hussain, J. Zhang, Y. Wang, "0-3 type Bi_3TaTiO_9: 40 wt% $BiFeO_3$ composite with improved high-temperature piezoelectric properties", *J. Alloys Compd.*, **740** (2018) 1–6.
18. Y. Yan, Z. Liu, Z. Li, M. Zhang, D. Zhang, Y. Feng, "Improving piezoelectric properties of $Pb(Ni,Nb)O_3$-$Pb(Hf,Ti)O_3$ ceramics by LiF addition", *Ceram. Int.*, **44** (2018) 5790–5793.
19. X. Xing, X. Zhu, J. Li, "Structure of $Pb(Zr,Ti)O_3$ (PZT) for power ultrasonic transducer", *J. Wuhan. University Technol. Mater.*, **33** (2018) 884–887.
20. M. Prabu, I.B.S. Banu, S. Gobalakrishnan, M. Chavali, "Electrical and ferroelectric properties of undoped and La-doped PZT (52/48) electroceramics synthesized by sol-gel method", *J. Alloys Compd.*, **551** (2013) 200–207.
21. J.S. Cross, K. Shinozaki, T. Yoshioka, J. Tanaka, S.H. Kim, H. Morioka, K. Saito, "Characterization and ferroelectricity of Bi and Fe co-doped PZT films", *Mater. Sci. Eng. B*, **173** (2010) 18–20.
22. U. Helbig, "Size effect in low grain size neodymium doped PZT ceramics", *J. Eur. Ceram. Soc.*, **27** (2007) 2567–2576.
23. C. Pientschke, A. Kuvatov, R. Steinhausen, H. Beige, R. Kruger, T. Muller, U. Helbig, D. Sporn, C. Schuh, S. Denneler, T. Richter, H. Schlich, "Bipolar strain hysteresis of poled composites with Nd-Mn-doped PZT fibres", *J. Eur. Ceram. Soc.*, **29** (2009) 1713–1720.
24. S.R. Shannigrahi, F.E.H. Tay, K. Yao, R.N.P. Choudhary, "Effect of rare earth (La, Nd, Sm, Eu, Gd, Dy, Er and Yb) ion substitutions on the microstructural and electrical properties of sol-gel grown PZT ceramics", *J. Eur. Ceram. Soc.*, **24** (2004) 163–170.
25. V. Kayasu, M. Ozenbas, "The effect of Nb doping on dielectric and ferroelectric properties of PZT thin films prepared by solution deposition", *J. Eur. Ceram. Soc.*, **29** (2009) 1157–1163.
26. Dipti, J.K. Juneja, S. Singh, K.K. Raina, C. Prakash, "Study on structural, dielectric, ferroelectric and piezoelectric properties of Ba doped lead zirconate titanate ceramics", *Physics B*, **431** (2013) 109–114.
27. C. Bedoya, C. Muller, J.L. Baudour, V. Madigou, "Sr-doped $PbZr_{1-x}Ti_xO_3$ ceramic: Structural study and field-induced reorientation of ferroelectric domains", *Mater. Sci. Eng. B*, **75** (2000) 43–52.
28. L. Yang, D.Y. Zheng, K.X. Guo, W.N. Zhao, Z.H. Peng, G.G. Peng, T. Zhou, "Mechanism of grain growth and excellent polarization, dielectric relaxtion of La^{3+}, Nd^{3+} modified PZT nano-films prepared by sol-gel technique", *J. Mater. Sci. Mater. Electron.*, **29** (2018) 18011–18019.
29. A. Dalakoti, A. Bandyopadhyay, S. Bose, "Effect of Zn, Sr, and Y addition on electrical properties of PZT thin films", *J. Am. Ceram. Soc.*, **89** (2006) 1140–1143.
30. T. Promjun, N. Funsueb, A. Ngamjarurojana, "Effect of Nb, Ta and Sb Addition on structure and electrical properties of PZT ceramics", *Mater. Today Proc.*, **17** (2019) 1602–1606.
31. Y. Matsuo, H. Sasaki, "Formation of lead zirconate-lead titanate solid solutions", *J. Am. Ceram. Soc.*, **48** (1965) 289–291.
32. X. Hao, J. Zhai, L.B. Kong, Z. Xu, "A comprehensive review on the progress of lead zirconate-based antiferroelectric materials", *Prog. Mater. Sci.*, **63** (2014) 1–57.
33. B. M. Song, D. Y. Kim, S.I. Shirasaki, H. Yamamura, "Effect of excess PbO on the densification of PLZT ceramics", *J. Am. Ceram. Soc.*, **72** (1989) 833–836.
34. M. Siddiqui, J.J. Mohamed, Z.A. Ahmad, "Structural, piezoelectric, and dielectric properties of PZT-based ceramics without excess lead oxide", *J. Austral. Ceram. Soc.*, **56** (2020) 371–377.
35. S. Samanta, M. Muralidhar, V. Sankaranarayanan, K. Sethupathi, M.S. Ramachandra-Rao, M. Murakami, "Band gap reduction and redshift of lattice vibrational spectra in Nb and Fe co-doped PLZT", *J. Mater. Sci.*, **52** (2017) 13012–13022.
36. E. Buixaderas, V. Bovtun, M. Kempa, D. Nuzhnyy, M. Savinov, P. Vanek, I. Gregora, B. Malic, "Lattice dynamics and domain wall oscillations of morphotropic $Pb(Zr,Ti)O_3$ ceramics", *Phys. Rev. B*, **94** (2016) 054315–054324.
37. Y. Chen, X. Bao, C.M. Wong, J. Cheng, H. Wu, H. Song, X. Ji, S. Wu, "PZT ceramics fabricated based on stereolithography for an ultrasound transducer array application", *Ceram. Int.*, **44** (2018) 22725–22730.
38. A. Meklid, S.E. Hachani, Z. Necira, H. Menasra, M. Abba, A. Boutarfaia, "Phase structure, microstructure and electrical properties of PCNS-PZ-PT ternary ceramics near the morphotropic phase boundary", *Appl. Phys. A*, **126** (2020) 32–38.
39. M.G. Garnica-Romo, A. Paez-Sanchez, L. Garcia-Gonzalez, I. Dominguez-Lopez, L.L. Diaz-Flores, M. Villicana-Mendez, "Nanoparticles of lead zirconate titanate (PZT) used as ferroelectric ceramics produced by sol-gel acetic-acid route", *J. Sol-Gel. Sci. Technol.*, **74** (2015) 425–431.
40. J. Wang, G. Wang, X. Chen, Z. Hu, H. Nie, F. Cao, X. Dong, "An investigation on phase transition behaviors in MgO-doped $Pb_{0.99}(Zr_{0.95}Ti_{0.05})_{0.98}Nb_{0.02}O_3$ ferroelectric ceramics by Raman and dielectric measurements", *Mater. Sci. Eng. B*, **193** (2015) 170–174.
41. W. Ji, B. Fang, X. Zhao, S. Zhang, X. Lu, J. Ding , "Enhancing electrical properties of high-Curie temperature piezoelectric ceramics BNT-PZT and their mechanism", *Curr. Appl. Phys.*, **19** (2019) 1367–1373.
42. M.C. Rodriguez-Aranda, F. Calderon-Pinar, M.A. Hernandez-Landaverde, J. Heiras, R. Zamorano-Ulloa, D. Ramirez-Rosales, J.M. Yanez-Limon, "Photoluminescence of sol-gel synthesized PZT powders", *J. Lumin.*, **179** (2016) 280–286.
43. F. Kahoul, L. Hamzioui, A. Guemache, M. Aillerie, A. Boutarfaia, "Study of dielectric and piezoelectric properties of (1-x)PZT-xSFN ceramics prepared by conventional solid state reaction method", *J. Chem. Soc. Pak.*, **42** (2020) 634–638.
44. M. Lorenz, G. Wagner, V. Lazenka, P. Schwinkendorf, H. Modarresi, M.J. Van-Bael, A. Vantomme, K. Temst, O. Oeckler, M. Grundmann, "Correlation of magnetoelectric coupling in multiferroic $BaTiO_3$-$BiFeO_3$ superlattices with oxygen vacancies and antiphase octahedral rotations", *Appl. Phys. Lett.*, **106** (2015) 012905–012909.
45. L. Bai, R. Gao, Q. Zhang, Z. Xu, Z. Wang, C. Fu, G. Chen, X. Deng, Y. Qiu, W. Cai, "Microstructure, dielectric and enhanced multiferroic properties of Fe_3O_4/$PbZr_{0.52}Ti_{0.48}O_3$ composite ceramics", *J. Mater. Sci. Mater. Electron.*, **30** (2019) 12295–12306.
46. T. Basu, S. Sen, A. Seal, A. Sen, "Temperature dependent

electrical properties of PZT wafer", *J. Electron. Mater.*, **45** (2016) 2252–2257.
47. L. Hamzioui, F. Kahoul, A. Boutarfaia, A. Guemache, M. Aillerie, "Structure, dielectric and piezoelectric properties of $Pb[(Zr_{0.45},Ti_{0.5})(Mn_{0.5},Sb_{0.5})_{0.05}]O_3$ ceramics", *Process. Appl. Ceram.*, **14** (2020) 19–24.